

Corrigendum to ‘Radiomic Prediction of CCND1 Expression Levels and Prognosis in Low-grade Glioma Based on Magnetic Resonance Imaging’ [Acad Radiol 2024;31:4595-4610]

Kun Zhao,¹ Hui Zhang,¹ Jianyang Lin, Shoucheng Xu, Jianzhi Liu, Xianjing Qian, Yongbing Gu, Guoqiang Ren, Xinyu Lu, Baomin Chen, Deng Chen, Jun Yan, Jichun Ma, Wenxiang Wei, Yuanwei Wang

The authors would like to inform you that the above-mentioned article is a Research article, but it was submitted and published as a Review article in error.

The authors apologise for any inconvenience caused by this mistake.

DOI of original article: <https://doi.org/10.1016/j.acra.2024.03.031>

Acad Radiol xxxx; xx:xxx-xxx

From the Department of Neurology, Affiliated People's Hospital of Jiangsu University, Zhenjiang, Jiangsu, China (K.Z., S.X., J.L.); Department of Cell Biology, Institute of Bioengineering, School of Medicine, Soochow University, Suzhou, Jiangsu, China (K.Z., W.W.); Suzhou Niumag Analytical Instrument Corporation, Suzhou, Jiangsu, China (K.Z., D.C., J.Y.); Fujian Center for Safety Evaluation of New Drug, Fujian Medical University, Fuzhou, Fujian, China (H.Z.); Department of General Surgery, Affiliated People's Hospital of Jiangsu University, Zhenjiang, Jiangsu, China (J.L.); Medical College, Jiangsu University, Zhenjiang, Jiangsu, China (X.Q.); Medical Imaging Department, Affiliated People's Hospital of Jiangsu University, Zhenjiang, Jiangsu, China (Y.G., G.R.); Department of Neurosurgery, Affiliated People's Hospital of Jiangsu University, Zhenjiang, Jiangsu, China (X.L., B.C.); Laboratory Center, Affiliated People's Hospital of Jiangsu University, Zhenjiang, Jiangsu, China (J.M.); Department of Neurology, Shuyang Hospital, Affiliated Shuyang Hospital of Xuzhou Medical University, Shuyang, Jiangsu, China (Y.W.). Received October 27, 2023; revised March 24, 2024; accepted March 24, 2024. **Address correspondence to:** Y.W.
e-mail: wyweilmn@126.com

¹ Kun Zhao and Hui Zhang contributed equally to this work.

Radiomic Prediction of CCND1 Expression Levels and Prognosis in Low-grade Glioma Based on Magnetic Resonance Imaging

Kun Zhao¹, Hui Zhang¹, Jianyang Lin, Shoucheng Xu, Jianzhi Liu, Xianjing Qian, Yongbing Gu, Guoqiang Ren, Xinyu Lu, Baomin Chen, Deng Chen, Jun Yan, Jichun Ma, Wenxiang Wei, Yuanwei Wang

Objectives: Low-grade glioma (LGG) is associated with increased mortality owing to recrudescence and the tendency for malignant transformation. Therefore, it is imperative to discover novel prognostic biomarkers as existing traditional prognostic biomarkers of glioma, including clinicopathological features and imaging examinations, are unable to meet the clinical demand for precision medicine. Accordingly, we aimed to evaluate the prognostic value of cyclin D1 (*CCND1*) expression levels and construct radiomic models to predict these levels in patients with LGG.

Materials and Methods: A total of 412 LGG cases from The Cancer Genome Atlas (TCGA) were used for gene-based prognostic analysis. Using magnetic resonance imaging (MRI) images stored in The Cancer Imaging Archive with genomic data from TCGA, 149 cases were selected for radiomics feature extraction and model construction. After feature extraction, the radiomic signature was constructed using logistic regression (LR) and support vector machine (SVM) analyses.

Results: *CCND1* was identified as a prognosis-related gene with differential expression in tumor and normal samples and plays a role in regulating both the cell cycle and immune response. Landmark analysis revealed that high-expression levels of *CCND1* were beneficial for survival ($P < 0.05$) in advanced LGG. Four optimal radiomics features were selected to construct radiomics models. The performance of LR and SVM achieved areas under the curve of 0.703 and 0.705, as well as 0.724 and 0.726 in the training and validation sets, respectively.

Conclusion: Elevated levels of *CCND1* expression could impact the prognosis of patients with LGG. MRI-based radiomics, especially the AUC values, can serve as a novel tool for predicting *CCND1* expression and understanding the correlation between elevated *CCND1* expression and prognosis.

Availability of Data and Materials: The datasets analyzed during the current study are available in the TCGA, TCIA, UCSC XENA and GTEx repository, <https://portal.gdc.cancer.gov/>, <https://www.cancerimagingarchive.net/>, <https://xenabrowser.net/datapages/>, <https://www.gtexportal.org/home/>.

Key Words: Low-grade glioma; *CCND1*/cyclin D1; Radiomics; Machine learning; Survival; Prognosis; Magnetic resonance imaging.

© 2024 The Association of University Radiologists. Published by Elsevier Inc. This is an open access article under the CC BY-NC-ND license (<http://creativecommons.org/licenses/by-nc-nd/4.0/>).

Acad Radiol xxxx; xx:xxx-xxx

From the Department of Neurology, Affiliated People's Hospital of Jiangsu University, Zhenjiang, Jiangsu, China (K.Z., S.X., J.L.); Department of Cell Biology, Institute of Bioengineering, School of Medicine, Soochow University, Suzhou, Jiangsu, China (K.Z., W.W.); Suzhou Niumag Analytical Instrument Corporation, Suzhou, Jiangsu, China (K.Z., D.C., J.Y.); Fujian Center for Safety Evaluation of New Drug, Fujian Medical University, Fuzhou, Fujian, China (H.Z.); Department of General Surgery, Affiliated People's Hospital of Jiangsu University, Zhenjiang, Jiangsu, China (J.L.); Medical College, Jiangsu University, Zhenjiang, Jiangsu, China (X.Q.); Medical Imaging Department, Affiliated People's Hospital of Jiangsu University, Zhenjiang, Jiangsu, China (Y.G., G.R.); Department of Neurosurgery, Affiliated People's Hospital of Jiangsu University, Zhenjiang, Jiangsu, China (X.L., B.C.); Laboratory Center, Affiliated People's Hospital of Jiangsu University, Zhenjiang, Jiangsu, China (J.M.); Department of Neurology, Shuyang Hospital, Shuyang Hospital Affiliated to Xuzhou Medical University, Shuyang, Jiangsu, China (Y.W.). Received October 27, 2023; revised March 24, 2024; accepted March 24, 2024. **Address correspondence to:** Y.W. e-mail: wyweilmn@126.com

¹ Kun Zhao and Hui Zhang contributed equally to this work.

© 2024 The Association of University Radiologists. Published by Elsevier Inc. This is an open access article under the CC BY-NC-ND license (<http://creativecommons.org/licenses/by-nc-nd/4.0/>).
<https://doi.org/10.1016/j.acra.2024.03.031>

INTRODUCTION

Gliomas are associated with poor prognosis, displaying high aggression, and are the most prevalent tumors in the central nervous system (1). According to the classification of gliomas (grade I–IV) by the latest 2021 World Health Organization (WHO) Classification of Tumors of the Central Nervous System (2), adult low-grade gliomas (LGGs, grades II and III), which harbor an isocitrate dehydrogenase (IDH) mutation and a 1p/19q-codeletion, grow slowly due to their low potential for malignant transformation (3). Current treatments include surgery, chemotherapy, radiotherapy, and immunotherapy. However, disability and mortality are relatively high owing to the recrudescence and tendency for malignant transformation (4,5). The classical prognostic biomarkers of gliomas are clinicopathological features, Ki67, IDH, and imaging examinations, such as computed tomography (CT) and magnetic resonance imaging (MRI). However, these biomarkers cannot satisfy the clinical demand for precision medicine. Therefore, new prognostic biomarkers must be identified, and patients must be stratified to identify novel indicators for individualized precision treatment.

Cyclin D1 (*CCND1*), the core gene of the cell cycle, is a frequently deregulated and relevant biomarker in certain tumors (6,7). During early G1 phase, *CCND1* functions as either a promoter of cell cycle progression from G1 to S phase (8) or as a growth factor sensor. Cyclin-dependent kinase 4/6 (CDK4/6) activity is required for the cell cycle G1/S transition. *CCND1* binds to CDK4/6 to form a complex, which can phosphorylate the tyrosine residue 172 of CDK4/6 and activate the kinase activity of CDKs (9). CDK4/6 inhibitors (CDK4/6i) act against tumors, restrain Rb phosphorylation, and prevent cell cycle progression from G1 to S phases (10). Consequently, the cells became senile and apoptotic. In clinical trials (<https://clinicaltrials.gov/ct2/home>), CDK4/6i was identified as a suitable treatment for gliomas. Hence, *CCND1* may be a prognostic or therapeutic biomarker for LGG.

Radiomics data are a high-throughput “image sequence” used to obtain a large number of imaging parameters, serving as a non-invasive, dynamic, and quantitative method to reflect tumor characteristics (11). CT, MRI, or digital radiography combined with other omics data and clinical characteristics into radiomics could benefit clinical decision-making. This approach can contribute to disease testing, assessment of therapeutic response, or determine a suitable conjecture for the possibility of disease progression and recurrence, death, and therapeutic schedule (12,13). Notably, radiogenomics is an emerging field that explores the relationship between genomics and radiomics (14,15). MAP-MRI could estimate the IDH 1/2 mutations, WHO grade 2/3, and chromosome 1p/19q combined deletion in adult-type diffuse gliomas (16). Using a deep learning method to analyze MRI radiomics data, researchers have confirmed that immunophenotype-associated mRNA signatures (IMriskScore) can offer personalized immunotherapy protocols and estimate the 1p/19q and IDH status (17) and patient prognosis (18–20). However, to date, studies demonstrating the use of radiomic features to predict *CCND1* expression levels are lacking.

Therefore, we aimed to explore the relationship between *CCND1* expression levels and the prognosis of patients with LGG using The Cancer Genome Atlas (TCGA) and The Cancer Imaging Archive (TCIA). Furthermore, based on MRI, we constructed radiomics models to predict *CCND1* expression levels, which could be used as a reference for clinical decisions and further studies.

METHODS

Study Design

This study was designed as a multi-factor exploratory study to probe and verify the heterogeneity of MRI radiomics features in LGG and reveal the underlying prognostic values of the biological mechanisms and heterogeneity (Fig 1).

Data Retrieval and Processing for This Study

Data for 199 LGG patients with enhanced MRI results (T1W1) were downloaded from TCIA database (www.cancerimagingarchive.net). The genomic data of 515 LGG patients were downloaded from TCGA database (portal.gdc.cancer.gov). Genomic data from 149 patients in TCGA were used to extract radiomic features and construct the model, and data from 412 patients were used to analyze the gene-based prognosis. The R package “survminer” (21) was used to divide patients into high- and low-expression groups using a cutoff value of 4.55 for *CCND1* expression. We prepared a radiomics model of *CCND1* and explored its prognostic value.

The exclusion criteria were samples without survival data, samples without clinical data, samples with survival time < 1 month, samples with poor image quality, and samples without enhanced T1W1 images. The inclusion criteria were as follows: samples of WHO grades II and III and samples with clinical and genomic data from TCGA. The detailed inclusion and exclusion criteria are shown in Table 1.

From UCSC XENA (xenabrowser.net/datapages), the obtained GBMLGG (glioma LGG) RNA sequencing (RNAseq) data in fragments per kilobase of transcript per million mapped fragments format were TCGA and GTEx (gtexportal.org/home) data processed by Using Toil flow unified (22). To compare the samples, the data were transformed to transcripts per million reads format via log₂ and demonstrated in a boxplot using the R package “ggplot2” (23).

Survival Analysis

Every variate was subjected to survival analysis using the R packages “survival” (24) and “survminer” (21). Using Kaplan–Meier (KM) survival curve analysis and the log-rank test, we showed the changes and significance of survival rates among the different groups. A survival rate of 50% was defined as the median survival time.

In the process of Cox regression and HR, the assumption of equal proportional risk should be satisfied, HR does not change

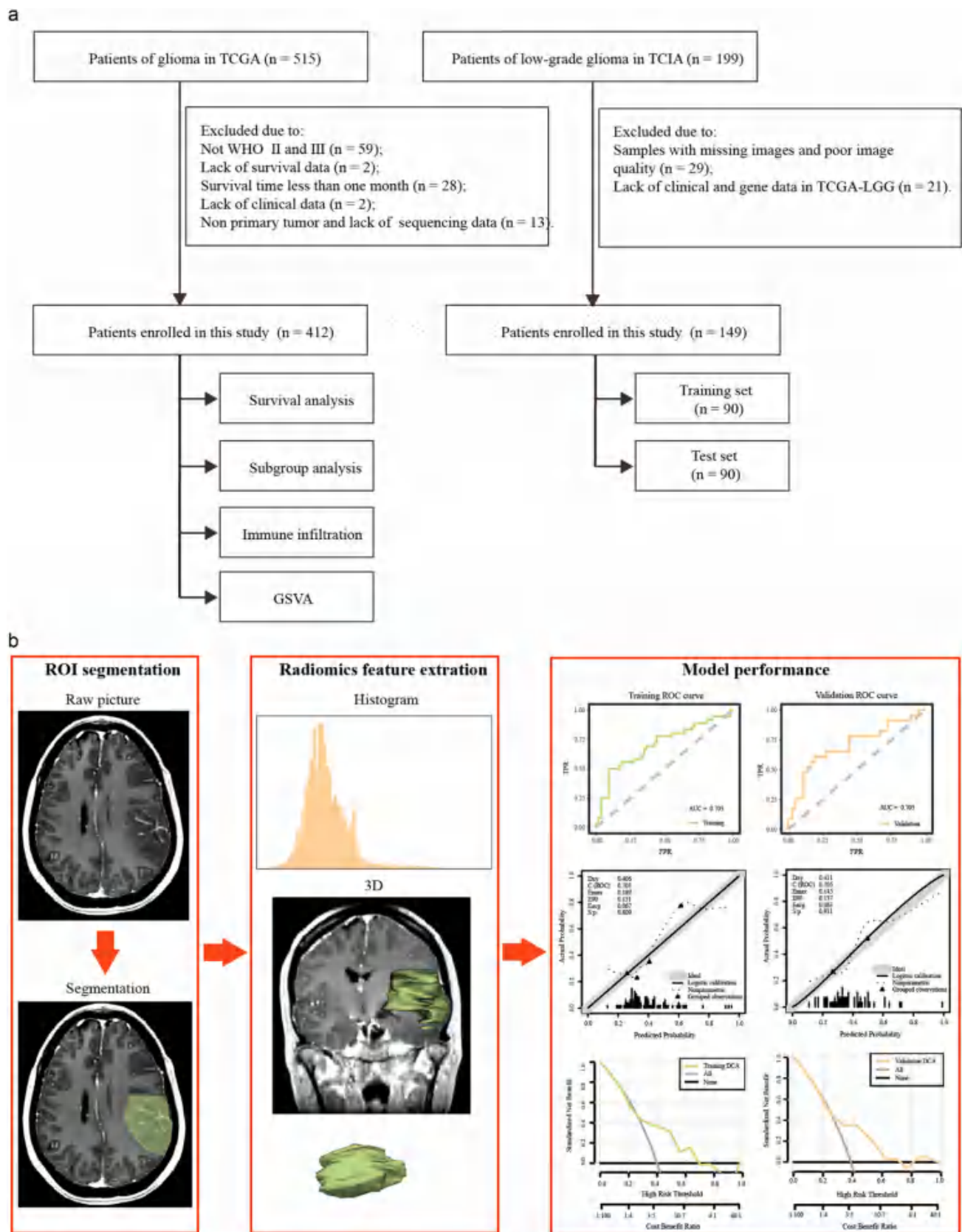


Figure 1. Workflow of this unsupervised analysis based on MRI radiomics features in the LGG patients. **(a)** Sample screening. **(b)** Radiomics analysis.

TABLE 1. Clinical Characteristics of the Population with High and Low CCND1 Expression Group

Variables	Total (n = 412)	Low (n = 242)	High (n = 170)	P value
Age, n (%)				1
~40	198 (48)	116 (48)	82 (48)	
41~	214 (52)	126 (52)	88 (52)	
Gender, n (%)				0.228
Female	183 (44)	101 (42)	82 (48)	
Male	229 (56)	141 (58)	88 (52)	
Histology, n (%)				0.684
Oligodendroglioma	158 (38)	93 (38)	65 (38)	
Astrocytoma	154 (37)	87 (36)	67 (39)	
Oligoastrocytoma	100 (24)	62 (26)	38 (22)	
Grade, n (%)				< 0.001*
WHO II	194 (47)	134 (55)	60 (35)	
WHO III	218 (53)	108 (45)	110 (65)	
IDH_status, n (%)				0.057
WT	80 (19)	55 (23)	25 (15)	
Mutant	332 (81)	187 (77)	145 (85)	
Chr_1p_19q_codeletion, n (%)				0.65
Non-Codel	273 (66)	163 (67)	110 (65)	
Codel	139 (34)	79 (33)	60 (35)	
MGMT_promoter_status, n (%)				0.024*
Unmethylated	73 (18)	52 (21)	21 (12)	
Methylated	339 (82)	190 (79)	149 (88)	
Chemotherapy, n (%)				0.001*
NO	173 (42)	118 (49)	55 (32)	
YES	239 (58)	124 (51)	115 (68)	
Radiotherapy, n (%)				0.24
NO	185 (45)	115 (48)	70 (41)	
YES	227 (55)	127 (52)	100 (59)	

* $P < 0.05$.

significantly over time. In reality, the failure of proportional risk assumption often occurs during long-term follow-up. For example, some treatments have good clinical benefits in the initial period but become less effective over time. Landmark analysis, a statistical analysis method, could be used to analyze a specific point in time in studies. Landmark analysis plotted the KM curve in time periods, comparing the “early stage”(from diagnosis to time node (12, 18, ..., 78, and 84 months)), and “late stage” (from time node to end of follow-up). In the KM curve analysis via landmarks, the abscissa is the survival time, and the ordinate is the mortality risk. Setting 12, 18, ..., 78, and 84 months as time nodes after diagnosis of LGG, we used the R packages “jskm” (CRAN.R-project.org/package=jskm) and “survival” (24) to plot a KM curve via landmark analysis. In addition, “early grade” was defined from diagnosis to time nodes, and “advanced grade” was defined from time nodes to the end of follow-up.

Univariate and Multivariable Cox Analysis

Cox proportional hazards regression can be used to explore the relationship between one factor or more factors and survival outcomes. We used univariate Cox regression to perform an association analysis to explore the factors influencing overall

survival (OS). Multivariate Cox regression was used to explore whether one independent factor or various factors would influence OS. To identify significant factors, all meaningful variables identified using univariate Cox regression analysis [hazard ratio (HR) < 1] were subjected to multivariate analysis. We used the R packages “survival” (24) and “forestplot” (CRAN.R-project.org/package=forestplot) for these analyses.

Subgroup Analysis and Interaction Test

Based on univariate Cox regression, we used exploratory subgroup analysis to analyze the impact of the main variable (high vs. low CCND1 expression) on patient prognosis in every covariate subgroup. Furthermore, we analyzed the interactions between CCND1 and other covariates using the log-likelihood ratio test. We used the “cmprsk,” “survival,” and “forestplot” R packages for these analyses.

Correlation Analysis

Based on Spearman’s rank correlation coefficient, we explored the correlation between CCND1 and clinical characteristics and presented the results using a correlation heat map.

The Correlation Between CCND1 Expression and Immune Cell Infiltration

The gene expression matrix of the LGG samples uploaded to the ImmuneCellAI database (bioinfo.life.hust.edu.cn/ImmuneCellAI/) was used to measure immune cell infiltration in each sample (25). Based on Spearman's rank correlation coefficient, we explored the correlation between CCND1 expression and immune cell infiltration and presented the results using a correlation heat map.

Gene Set Variation Analysis (GSVA) Between Low and High CCND1 Expression

GSVA is a non-parametric, unsupervised analysis method to evaluate gene set enrichment in microarrays and transcriptomes (26). Based on the KEGG pathways and hallmark gene sets, GSVA was used to calculate the pathway enrichment score for each of the 412 LGG samples from TCGA-LGG. The R package "limma" (27,28) was used for differential analysis of low and high CCND1 expression.

Segmentation and Radiomics Feature Extraction

By using the open-source software 3D Slicer, the MRI images were delineated through the Digital Imaging and Communications in Medicine (DICOM) format. Two experienced radiologists reviewed all magnetic resonance imaging (MRI) scans independently to delineate the regions of interest (ROIs) slice-by-slice manually on enhanced MRI images. N4 bias field correction was employed on the MRI image to mitigate the impact of bias fields caused by the uneven signal intensity in the MRI image.

Before radiomic feature extraction, we resampled the voxel size of the VOI to $1 \times 1 \times 1 \text{ mm}^3$ by way of the cubic interpolation to shorten feature value variability. Altogether, 107 radiomics factors (RFs), including first-order and texture features (original), square root, shape, wavelet, exponential, log, square, lbp, logarithm and gradient features were extracted for model construction and further analysis, using the open-source software ("pyradiomics" python package) (29). Based on the CCND1 threshold value (4.554), samples were divided into low- and high-expression groups. By intersecting TCGA transcriptome data and TCIA radiomics data, 149 TCGA-TCIA intersection samples were standardized via "pyradiomics". Next, using the R packages "caret" and "CBCgrps" (30), we divided the data into training and validation sets randomly at a ratio of 6:4 and analyzed the difference between them via z-score standardization (i.e., mean 0 and standard deviation 1).

Feature Selection

The maximum relevance, minimum redundancy (mRMR) screening feature considers the correlations between the features and the predicted variables, as well as the correlation between the features themselves. The metric used was mutual information. For the mRMR method, the correlation between feature subsets and categories was calculated as the

mean of the information gain of each feature and category, while the redundancy among features was calculated as the sum of the mutual information among features divided by the square of the number of features in the subset.

Relief, a well-known filtration feature selection method, is a feature-weighting algorithm that ensures different weights for each feature according to its relevance and class. Features are removed when the weight is below a certain threshold. In the relief algorithm, the correlation between features and categories is based on the strength of the ability to distinguish close samples based on features. The larger the weight of the feature, the stronger its classification ability; conversely, a lower weight indicates a weaker classification ability.

To eliminate redundant radiomic features, we used the mRMR and Relief methods to optimize the feature selection.

Construction of the Radiomics Model

Based on variations in linear regression, the logistic regression (LR) model is a generalized regression algorithm widely used in classification. The R package 'stats' was used to fit the screened radiomic features using the LR algorithm to construct a model for predicting gene expression.

Support vector machines (SVMs) with a Gaussian kernel were employed in the reduced feature space as the classifiers of choice to discriminate the two cohort groups. The rationale for adopting SVMs as classifiers is primarily due to their ability to generate classification hyperplanes, so the margins between the hyperplane and the nearest instances of the classified sample categories are maximized. The basic principle of SVM is to divide different categories of data by finding a hyperplane in the data space. The selection of this hyperplane requires maximizing the distance from the support vector to the hyperplane, that is, maximizing the width of the classification boundary. The R packages "stats" and "caret" were, respectively, used to fit the screened radiomics features with the LR algorithm and SVM to construct a model for predicting gene expression.

The radiomics model was evaluated using training and validation sets. The evaluation indexes were accuracy, specificity, sensitivity, positive predictive value, and negative predictive value. The x-axis of the receiver operating characteristic curve was the false-positive rate, whereas the y-axis was the true-positive rate. A larger area under the curve (AUC) and a more convex curve to the upper-left corner indicated a better model effect. Calibration of the radiomics prediction model was evaluated by drawing the calibration curve and performing the Hosmer-Lemeshow goodness-of-fit test. The Brier score was used to quantify the comprehensive performance of the radiomic prediction model. A Brier score closer to 0 indicated more consistent model prediction. The degree of clinical benefit of the radiomic prediction model was determined by drawing a decision curve (DCA). The DeLong test was used to compare the AUC values of the training and validation sets to determine the condition of fit. The radiomics model score was used to

predict the probability of gene expression. A Wilcoxon test was used to compare the radiomics scores (RSs) between the high and low *CCND1* expression groups.

Intraclass Correlation Coefficient (ICC)

ICC was used to evaluate the consistency of radiomic features extracted from volume of interest delineated by two radiologists (31). First, one radiologist delineated all patient images. Another radiologist delineated 20 randomly selected samples and extracted the radiomics features. $ICC \geq 0.80$ was typically considered an optimal agreement; $0.51\text{--}0.79$, considered moderate agreement; and < 0.50 , considered poor agreement (31). The correlation between *CCND1* and immune-related genes was analyzed based on SVM model prediction.

Statistical Analysis

All statistical analyses were conducted using R version 4.0.0 (<https://www.r-project.org>). $P < 0.05$ was considered statistically significant.

RESULTS

Patient Characteristics

A total of 412 patients from TCGA were included in this study; among them, 170 patients belonged to the high *CCND1* expression group and 242 patients to the low *CCND1* expression group. The baseline clinical data of the two groups were compared (Table 1). We observed that WHO grade ($P < 0.001$), 6-oxo-methylguanine DNA methyltransferase (MGMT) promoter status ($P = 0.024$), and chemotherapy ($P = 0.001$) had a significant difference, whereas age, sex, and IDH status had no significance ($P \geq 0.05$).

Differences and Survival Analysis of *CCND1* and Clinical Features

First, compared to normal tissues, *CCND1* expression was significantly higher ($P < 0.001$) in LGG tissues (Fig 2a). The median survival time was 81.1 and 76.2 months for patients with low and high *CCND1* expression, respectively. The KM results demonstrated that a high *CCND1* expression level was related to OS in most curves, but this was not statistically significant ($P = 0.117$) (Fig 2b). However, 12, 18,, 78, or 84 months after diagnosis was used as a landmark, and univariate landmark analysis of survival was used to assess the survival difference between the early- and late-period LGG. The KM curve demonstrated that when 78 or 84 months were used as landmarks, there was no significant difference between the low- and high-*CCND1* group ($P < 0.05$) in the early period, but the difference in the later period was significant ($P < 0.05$) (Fig 2c–d). Thus, *CCND1* mainly affects LGG development in the later period.

We further explored whether the clinical features had an effect on patient survival. We found that only WHO grade was significantly related to OS ($P = 0.029$) (Fig 2e).

Univariate and Multivariate Cox Regression Analysis

Univariate Cox regression analysis revealed that high *CCND1* expression was a protective factor for OS (HR = 0.729, 95% CI: 0.491–1.084), but no significant correlation was observed ($P = 0.118$). The grade was a risk factor for OS (HR = 1.54, 95% CI: 1.042–2.278), and a significant correlation was observed between grade and clinical outcomes ($P = 0.03$). However, both *CCND1* and tumor grade were independent positive prognostic factors in multivariate Cox regression analysis ($P < 0.05$). The other covariates were not significantly correlated with clinical outcomes (Fig 3a).

Subgroup Analysis and Interactive Effect

Subgroup analysis was performed to explore the influence of the covariates. In WHO grade II, high *CCND1* expression was a protective factor for OS (HR = 0.862, 95% CI: 0.402–1.847); however, we observed no significant correlation ($P = 0.7$). Nevertheless, in WHO grade III, high *CCND1* expression was a protective factor for OS (HR = 0.555, 95% CI: 0.343–0.898), which was significantly correlated with clinical outcomes ($P = 0.016$). In WHO grade III, tumor grade had no significant interactive effect on the correction of *CCND1* and OS in LGG patients ($P = 0.38$). Other covariates had no significant correlation with clinical outcomes, nor did they have an interactive effect on the correction of *CCND1* and OS (Fig 3b).

Correlation Between *CCND1* and Clinical Features

Counterintuitively, *CCND1* expression level correlated positively with chemotherapy ($P < 0.01$), grade ($P < 0.01$), IDH status ($P < 0.05$), MGMT promoter status ($P < 0.05$), and radiotherapy ($P < 0.05$) in LGG.

Correlation Between *CCND1* and Immune Infiltration

As demonstrated in Figure 5, 11 immune cell types showed significance in the correlation analysis between *CCND1* and immune infiltration ($P < 0.05$). Specifically, natural killer T, gamma delta T, central memory, and effector memory cells were positively correlated with *CCND1* ($\text{cor} > 0$). Alternatively, B cells, Tr1 cells, monocytes, DCs, $CD4^+$ T cells, iTregs, and exhausted cells were negatively correlated with *CCND1* expression ($\text{cor} < 0$).

Gene Set Variation Analysis

Based on the high and low *CCND1* expression levels in LGG, we analyzed the enrichment of DEGs. In the KEGG gene set (Fig 6a), we observed significant enrichment of pathways such as the PPAR signaling pathway among samples with high *CCND1* expression. Conversely, low

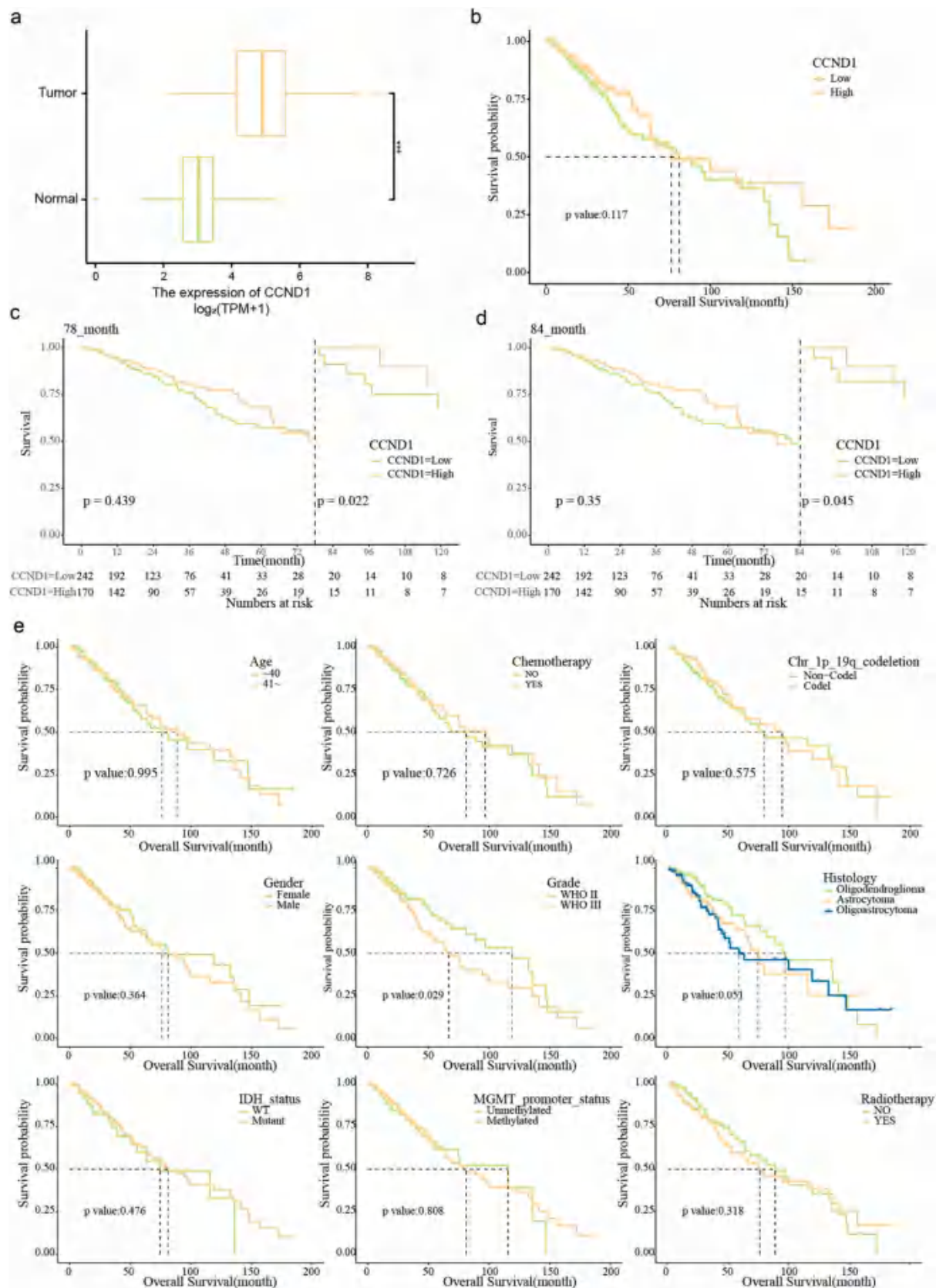


Figure 2. Comparison of the CCND1 and survival analysis of CCND1 and clinical features. **(a)** Difference of CCND1 expression between normal tissues in GTEx and LGG tissues in TCGA. **(b)** survival analysis of high- and low- expression of CCND1. **(c-d)** Univariate landmark analysis of high- and low- expression of CCND1. **(e)** survival analysis of clinical features (age, chemotherapy, Grade, etc.) of LGG. * $P < 0.05$, ** $P < 0.01$, *** $P < 0.001$.

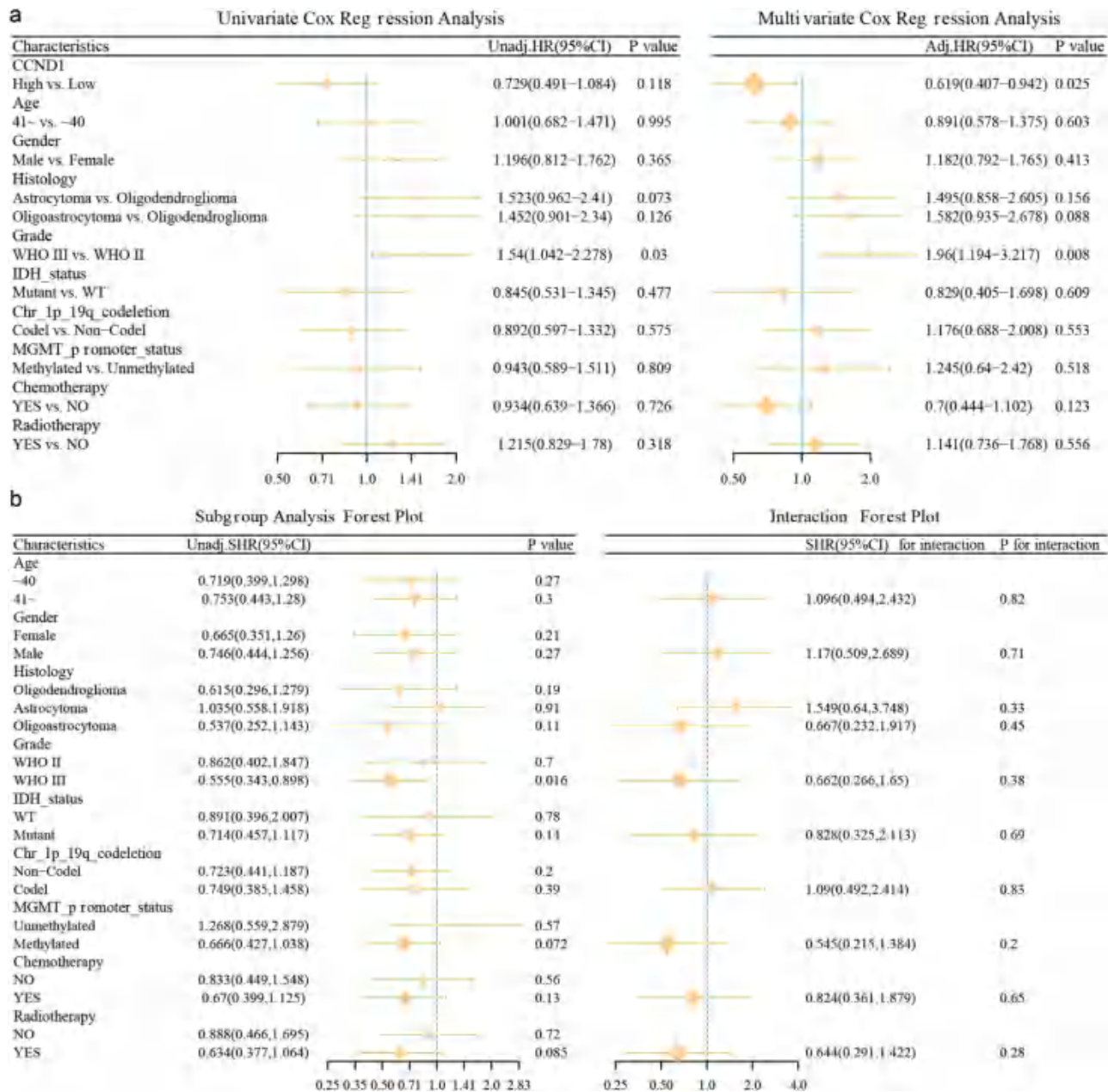


Figure 3. Forest plot of Cox regression analysis, subgroup analysis and interaction. **(a)** Forest plot of Univariate and multivariate Cox regression analysis. The model incorporated the CCND1, Grade, age, gender, histology, IDH_status, 1p-19q, MGMT, Chemotherapy, and Radiotherapy. When demonstrating the HR of CCND1, we had adjusted the other factors excluding CCND1; and when demonstrating the HR of Grade, we had adjusted the other factors excluding Grade. **(b)** Forest plot of subgroup analysis and interaction. * $P < 0.05$, ** $P < 0.01$.

CCND1 expression was associated with significant enrichment in pathways related to, cell cycle and DNA repair, among others. In the hallmark gene set (Fig 6b), we observed that high CCND1 expression significantly enriched the KRAS signaling pathway, while low expression of CCND1 was associated with significant enrichment in pathways related to DNA repair and E2F target signaling. Overall, in both the KEGG and hallmark gene sets, low expression of CCND1 significantly enriched seven signaling pathways: apoptosis, DNA repair, MTORC1 signaling, Notch

signaling, p53 pathway, TGF beta signaling, and WNT/beta-catenin signaling.

Clinicopathologic Characteristics of Participants Involved in Radiomics Analysis

Radiomics Feature Extraction, Model Establishment Consistency Evaluation, Feature Selection, and Construction of the Radiomics Model

Using PyRadiomics (29), we performed radiomics feature extraction and ICC. The interobserver ICC was ≥ 0.8 , 0.5–0.79,

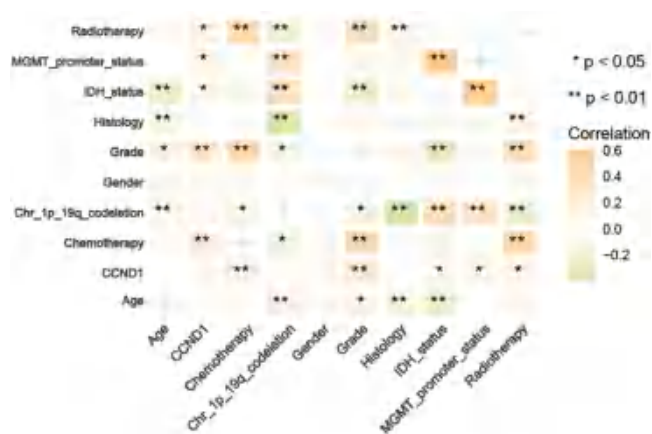


Figure 4. Correlation analysis between CCND1 and clinical features in LGG. Light orange represents positive correlation, light green represents negative correlation. * $P < 0.05$, ** $P < 0.01$. (Color version of figure is available online.)

and < 0.5 for 91, 15, and 1 of the features, respectively. Subsequently, using mRMR and the relief algorithm, we performed the top 20 features, and obtained five features (ngtdm_Busyness, firstorder_Kurtosis, glcm_Imc2, glszm_SizeZoneNonUniformity, ngtdm_Complexity) by intersection

(Fig 7, Table 3). The data were divided into training (90) and verification (59) sets. In the analysis of differences in each variable between groups, $P > 0.05$ indicated comparability between the training and validation sets (Table 2).

In the training set, the radiomics model was constructed using the LR algorithm and used to analyze the importance of the selected features (Fig 8a, Table 3), whose ICC values were all > 0.8 , with good consistency. Subsequently, the receiver operating characteristic curve was used to evaluate the radiomics model, and the AUC values were 0.703 and 0.705 for the training and validation sets, respectively (Fig 8b–c). We compared the AUC values between the training and validation sets and found no significant differences ($P = 0.978$). Furthermore, the calibration curve analysis and Hosmer–Lemeshow goodness-of-fit were consistent with the true values ($P > 0.05$) (Fig 8d–g). The DCA model demonstrated clinical practicability. In addition, compared with the low CCND1 expression group, the high CCND1 expression group was significantly higher ($P < 0.01$) in both the training and validation sets (Fig 8h–i).

To determine the reliability of the radiomics model, we used the SVM algorithm to conduct radiomics and analyze the importance of the selected features (Fig 9a, Table 3). In the training and validation sets, AUC values were 0.724 and 0.726, respectively, (Fig 9b–c), which were higher than those in the LR. We

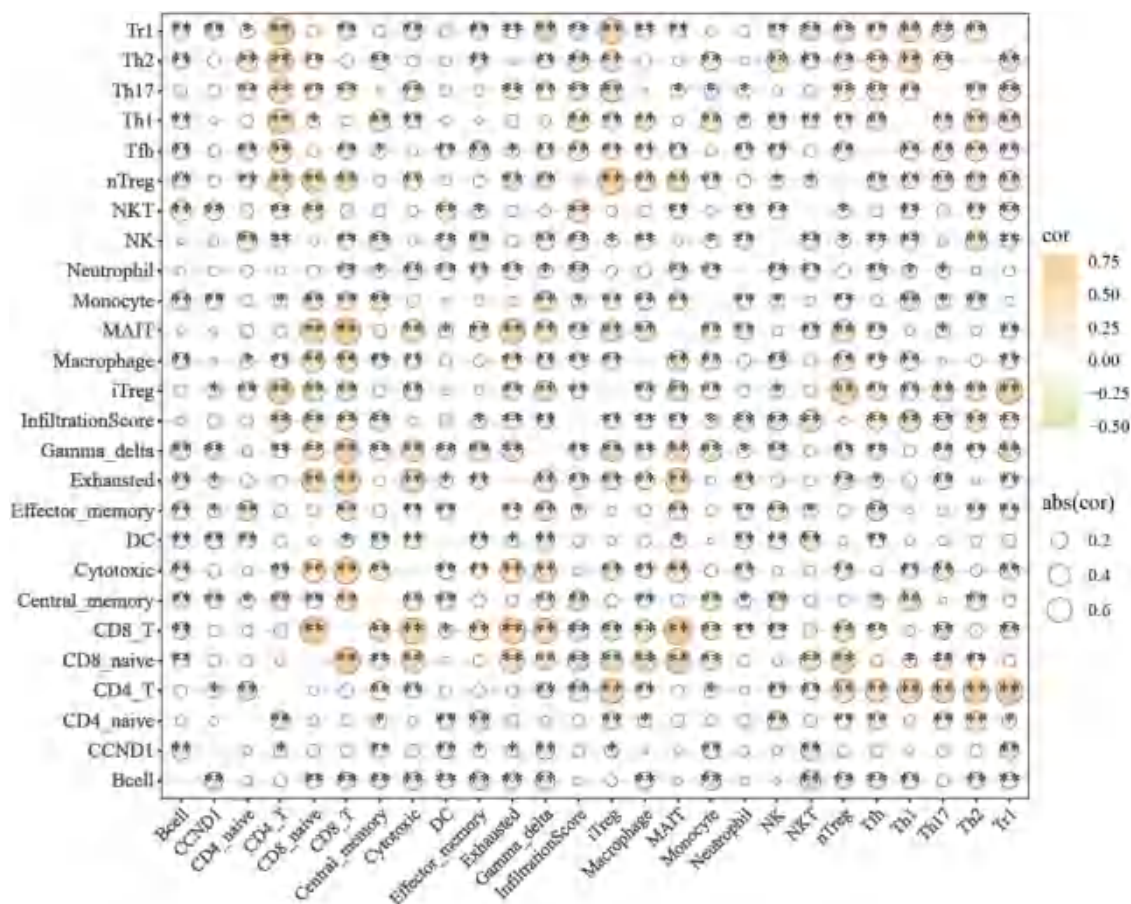


Figure 5. Correlation analysis between CCND1 and immune infiltration in LGG in the ImmuCellAI database. Light orange represents positive correlation, light green represents negative correlation. * $P < 0.05$, ** $P < 0.01$. (Color version of figure is available online.)

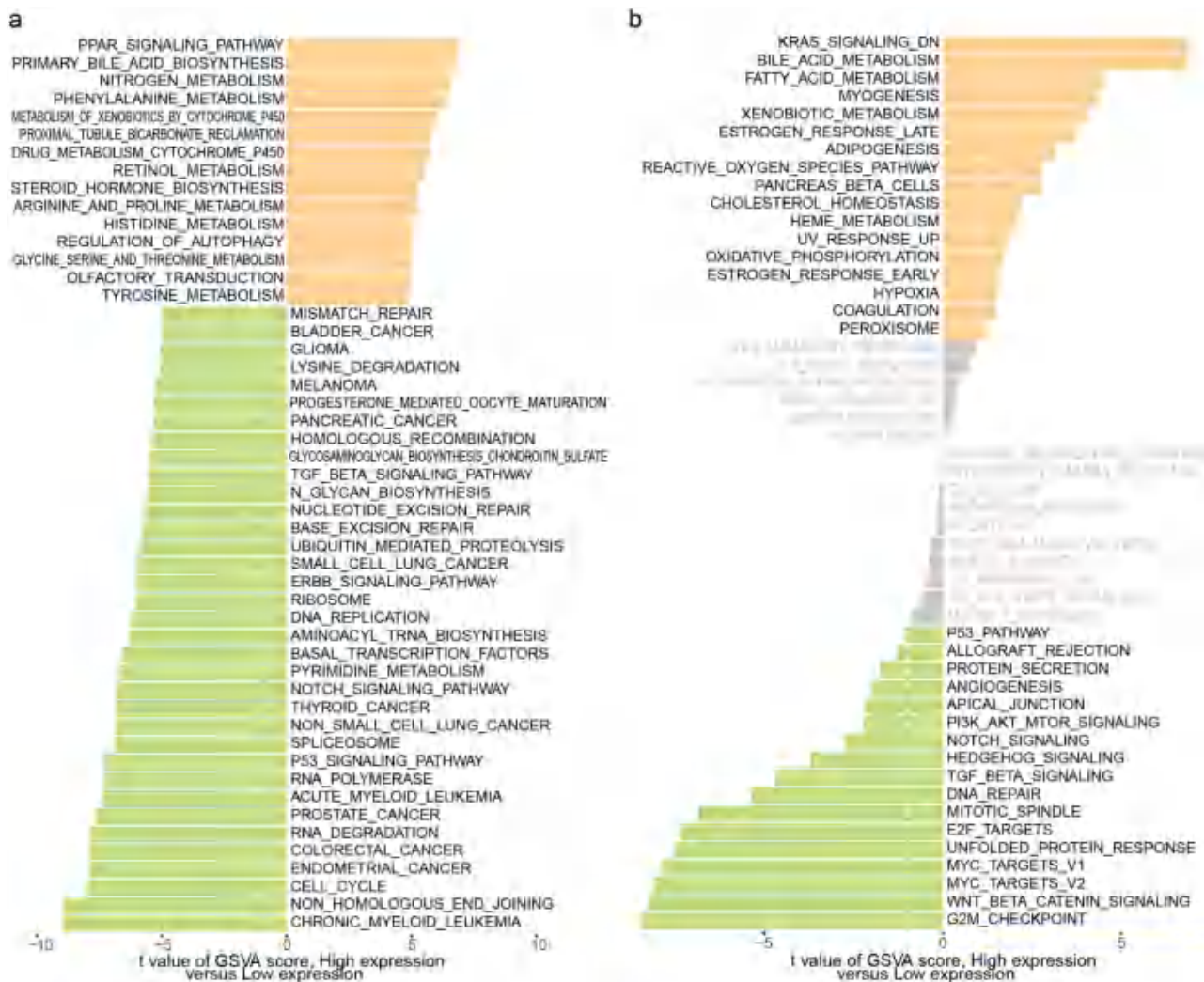


Figure 6. GSVA (gene set variation analysis). **(a)** GSVA in KEGG gene set. **(b)** GSVA in Hallmarker gene set. Light orange represents positive correlation, light green represents negative correlation. (Color version of figure is available online.)

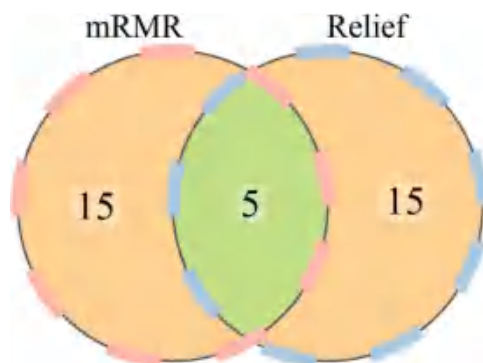


Figure 7. Features selection.

also compared the AUC values between the training and validation sets and found no significant differences ($P=0.986$). Furthermore, we observed equivalent predictions of the two models by comparing the AUC values between the LR and SVM in the training and validation sets ($P=0.153, 0.346$).

Furthermore, the calibration curve analysis and Hosmer–Lemeshow goodness-of-fit were consistent with the true values ($P > 0.05$) (Fig 9d–g). The DCA model demonstrated clinical practicability. In addition, compared with the low *CCND1* expression group, the high-expression group was significantly higher in both the training and validation sets ($P < 0.001, 0.01$, respectively) (Fig 9h–i). In summary, the radiomics model predicted by the SVM was superior to that predicted by LR.

Correlation of Radiomics Model with *CCND1* and Immune-Related Genes

As shown in Figure 10 and Table 4, *CCND1* was positively correlated with RS ($\text{cor} = 0.36, P < 0.001$), and nine genes were significantly correlated with *CCND1* and immune-related genes ($P < 0.05$). Namely, *CD28*, *TNFRSF9*, *LAG3*, *CD276*, and *NRP1* were positively correlated with *CCND1* expression ($\text{cor} > 0$). Additionally, *HHLA2*, *TNFRSF14*, *CD200R1*, and *ICOSLG* were negatively correlated with *CCND1* ($\text{cor} < 0$). Three genes were significantly correlated

TABLE 2. Clinical Characteristics of the Population with High and Low Radiomics Score Groups

Variables	Total (n = 149)	Train (n = 90)	Validation (n = 59)	P value
CCND1, n (%)				1
Low	90 (60)	54 (60)	36 (61)	
High	59 (40)	36 (40)	23 (39)	
Age, n (%)				0.54
~40	69 (46)	44 (49)	25 (42)	
41~	80 (54)	46 (51)	34 (58)	
Gender, n (%)				0.892
Female	76 (51)	45 (50)	31 (53)	
Male	73 (49)	45 (50)	28 (47)	
Histology, n (%)				0.528
Astrocytoma	50 (34)	30 (33)	20 (34)	
Oligoastrocytoma	34 (23)	18 (20)	16 (27)	
Oligodendroglioma	65 (44)	42 (47)	23 (39)	
Grade, n (%)				0.348
WHO II	75 (50)	42 (47)	33 (56)	
WHO III	74 (50)	48 (53)	26 (44)	
IDH_status, n (%)				0.735
Mutant	117 (79)	72 (80)	45 (76)	
WT	32 (21)	18 (20)	14 (24)	
Chr_1p_19q_codeletion, n (%)				0.244
Codel	42 (28)	29 (32)	13 (22)	
Non-Codel	107 (72)	61 (68)	46 (78)	
MGMT_promoter_status, n (%)				1
Methylated	119 (80)	72 (80)	47 (80)	
Unmethylated	30 (20)	18 (20)	12 (20)	
Chemotherapy, n (%)				0.421
NO	56 (38)	31 (34)	25 (42)	
YES	93 (62)	59 (66)	34 (58)	
Radiotherapy, n (%)				0.712
NO	57 (38)	36 (40)	21 (36)	
YES	92 (62)	54 (60)	38 (64)	
OS, n (%)				1
Alive	119 (80)	72 (80)	47 (80)	
Dead	30 (20)	18 (20)	12 (20)	
OS.time, Median (Q1,Q3)	22.37 (13.8, 40.43)	20.83 (13.83, 37.81)	24.13 (13.23, 46.12)	0.357

with RS and immune-related genes ($P < 0.05$). *TNFRSF8*, *TNFRSF9*, and *CCND1* were positively correlated with *CCND1* ($\text{cor} > 0$). In addition, *TIGIT* was negatively correlated with *CCND1* ($\text{cor} < 0$). We observed that *TNFRSF9* was correlated with *CCND1* ($\text{cor} = 0.24$, $P < 0.01$), as well as with RS ($\text{cor} = 0.30$, $P < 0.001$).

DISCUSSION

We evaluated *CCND1* expression levels and their clinical prognostic value in patients with LGG by analyzing MRI images in the TCIA database. Our results demonstrated that MRI features are associated with differences in *CCND1* expression levels in LGG, implying that supererogatory gene information could be explored from radiomics analysis of MRI images. The machine learning models improved accuracy by incorporating clinical and radiomic MRI parameters.

Owing to the LGG subtype, the median OS ranges from 11.7 to 19.9 years (32); thus, further prognostic information must be considered. According to the 6th edition of the WHO classification of central nervous system tumors (2), a comprehensive and integrated diagnosis of LGG necessitates a combination of diagnostic features drawn from relevant histological, immunochemical, molecular, and other abnormalities. Silencing *CCND1* may benefit liver cancer therapy, serving as a marker for liver cancer stem cells (33,34). Moreover, *CCND1*, which may promote tumor development and regeneration, has been actively investigated in various types of tumors, including breast, melanoma, bladder, and thyroid cancer (9,35–38). The *CCND1* G870A polymorphism has been associated with a potentially increased risk of gliomas in the Chinese population (39). Our research focused on the significance and role of *CCND1* in LGG. We found that high *CCND1* expression levels are linked to poorer prognosis in patients with advanced LGG

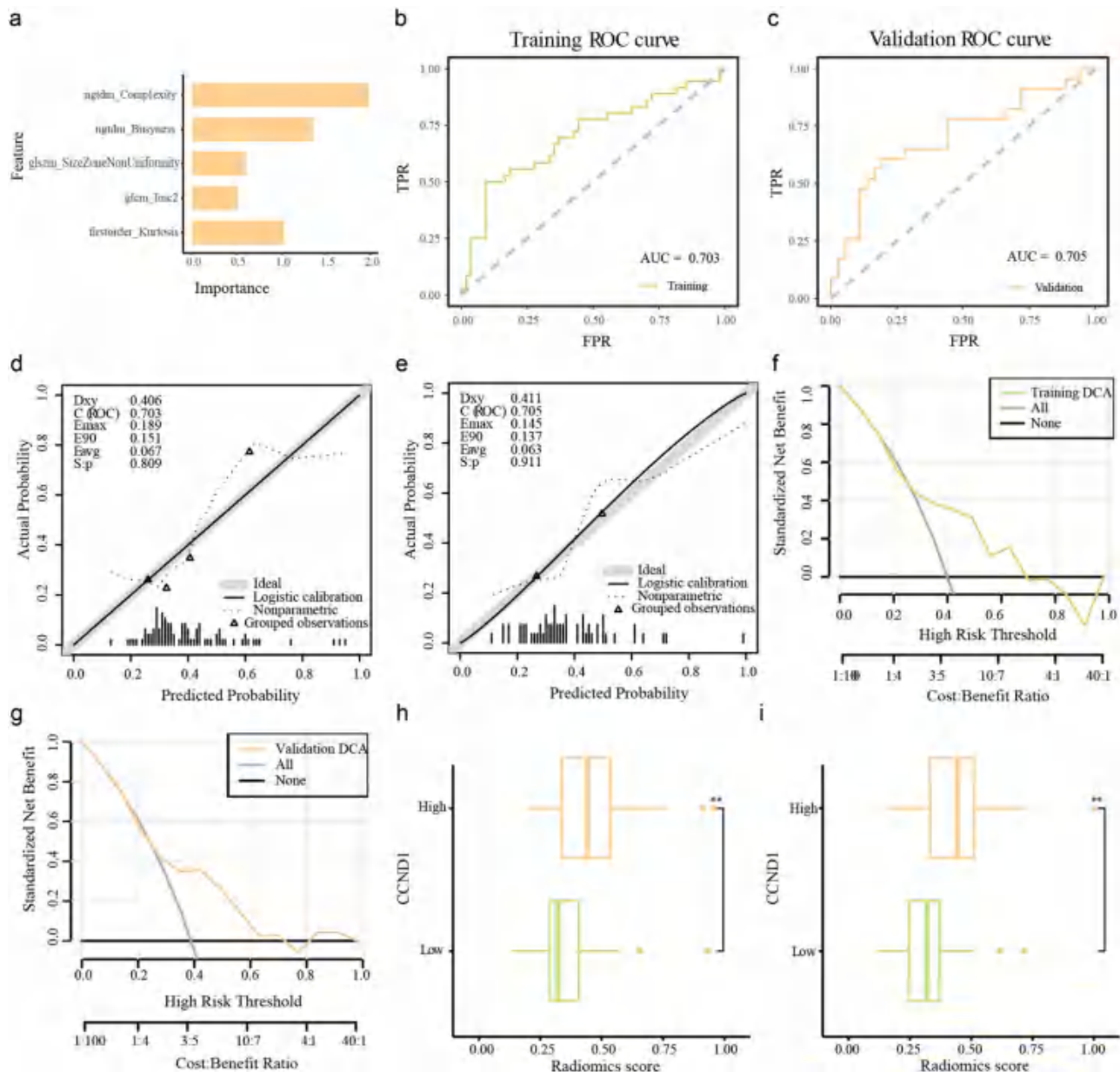


Figure 8. Construction and evaluation of the LR radiomics models. **(a)** Importance of the selected features in the model. **(b–c)** ROC curve analysis of the radiomics model. **(d–e)** Calibration-curve analysis of the radiomics model. **(f–g)** Hosmer–Lemeshow goodness-of-fit testing of the radiomics model. **(h–i)** Association between RS and CCND1 expression. Light orange represents positive correlation, light green represents negative correlation. * $P < 0.05$, ** $P < 0.01$, *** $P < 0.001$. (Color version of figure is available online.)

TABLE 3. Radiomics Features

Item	Importance
<i>ngtdm_Busyness</i>	1.353484245
<i>firstorder_Kurtosis</i>	1.031935343
<i>glcm_Imc2</i>	0.518207678
<i>glszm_SizeZoneNonUniformity</i>	0.606335873
<i>ngtdm_Complexity</i>	1.983987285

($P < 0.05$) using landmark analysis of 412 samples from TCGA. Furthermore, we demonstrated that *CCND1* expression is correlated with chemotherapy, tumor grade,

IDH_status, MGMT_promoter_status, and radiotherapy. Thus, an in-depth study of the role of *CCND1* in LGG could be important to patient therapy.

MRI, a method that lacks objectivity and quantification, depends on morphological characteristics for diagnosis. Radiomics /can minimize high-throughput data from medical images, recognize deep information that cannot be observed with the naked eye, and perform quantitative analyses. By distilling the MRI image features in bladder cancer using radiomics, the AUC of the predictive model for muscle invasion was 0.920 in the training cohort and 0.844 in the test cohort (40). According to dynamic contrast

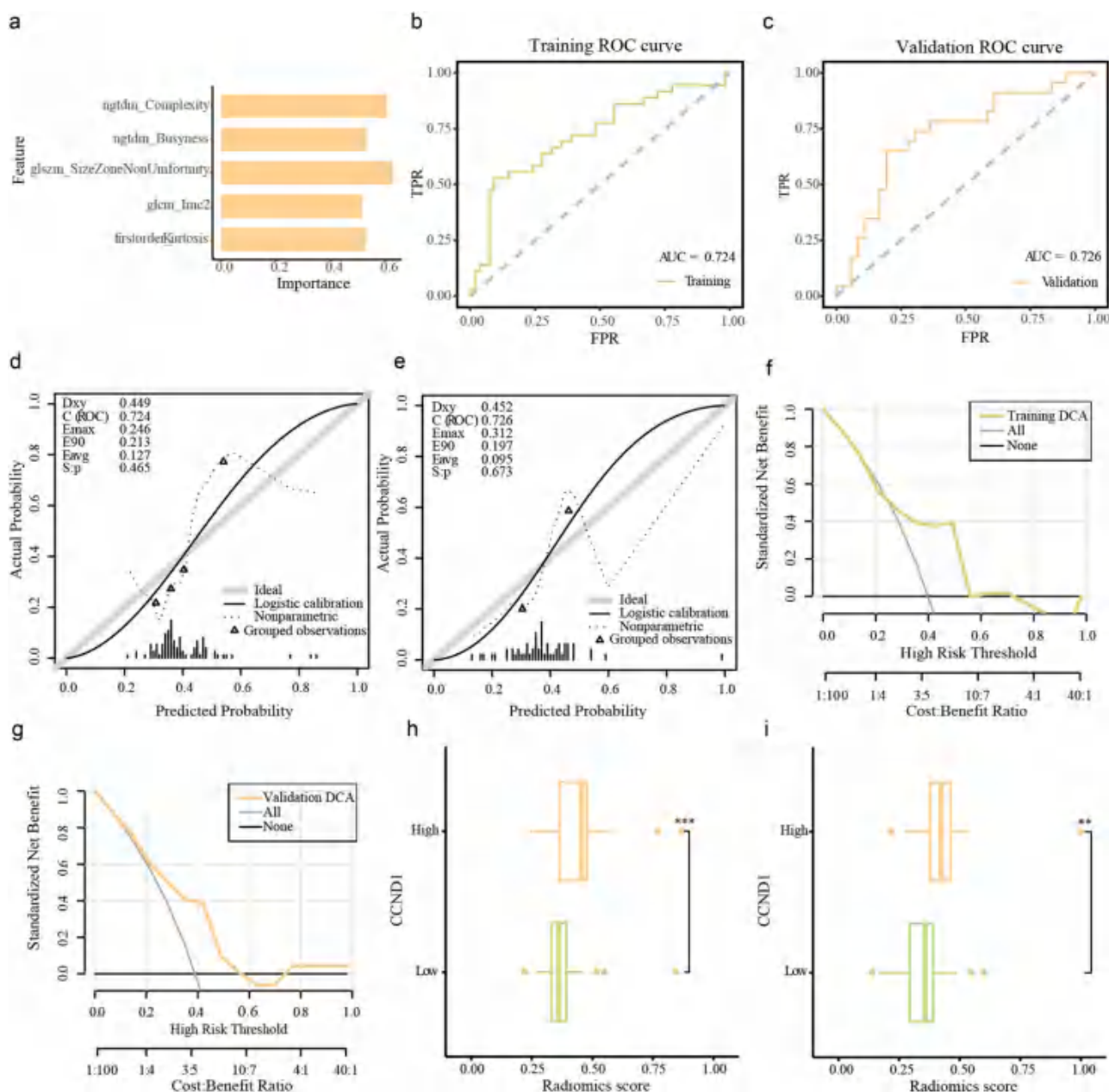


Figure 9. Construction and evaluation of the SVM radiomics models. **(a)** Importance of the selected features in the model. **(b-c)** ROC curve analysis of the radiomics model. **(d-e)** Calibration-curve analysis of the radiomics model. **(f-g)** Hosmer–Lemeshow goodness-of-fit testing of the radiomics model. **(h-i)** Association between RS and CCND1 expression. Light orange represents positive correlation, light green represents negative correlation. * $P < 0.05$, ** $P < 0.01$, *** $P < 0.001$. (Color version of figure is available online.)

enhanced-MRI and apparent diffusion coefficient maps, radiomics features can be used as imaging biomarkers to confirm Ki-67 status in patients with breast cancer (41). Based on multi-parametric MRI, a radiomic nomogram can predict the tumor grade to guide the dilation and surgery model in endometrial cancer (42). The multi-layer perceptron model, including clinical features, mutation status of the epidermal growth factor receptor, and radiomics, effectively predicted the risk of death, which can promote the individualized management of patients with lung cancer and brain metastases (43). However, we referred to existing

models of LGG. The AUC of 14 gene signatures was greater than 0.70 for survival rates (1-, 3-, 5-year) (44). The AUC of risk score based on CIA-II (anti-silencing function 1 B) was greater than 0.70 for survival rates (1-, 3-, 5-year) (45). The AUC of ZNF480 (Zinc Finger Protein 480) was greater than 0.59 (46). We observed that the AUC scores of model prediction were not exceptionally high, with values exceeding 0.70 considered relatively convincing. In the present study, based on low and high CCND1 expression levels, five radiomic features were selected via mRMR and relief to construct the LR and SVM models. In both models, the



Figure 10. Correlation analysis of RS, CCND1 expression, and expression of immune genes expression. * $P < 0.05$, ** $P < 0.01$, *** $P < 0.001$, **** $P < 0.0001$.

AUC of the radiomics features was > 0.70 ; moreover, both LR and SVM exhibited acceptable consistency and diagnostic efficacy. Furthermore, our study based on MRI was low-cost, replicate, and non-invasive. Collectively, these findings suggest that the combination of radiomics and molecular features will be a trend for future research.

Based on radiomics features and clinical characteristics, Chen et al. (47) built a combined survival model to help patients with advanced gastric cancer in future clinical decision-making. Boot et al. (48) developed a predictive model to forecast human papillomavirus status with acceptable performance and improve survival prediction. Ming et al. (49) observed that imaging subtypes might serve as potential biomarkers. Wan et al. (50) demonstrated the radiographic models, based on radiomic and radiographic features, gave evidence of predicting DNA copy-number, especially DNA copy-number 2. In this study, we built prognostic models based on clinical and radiomics features for survival analysis of patients with LGG. Landmark analysis revealed that the

high *CCND1* expression group in advanced LGG significantly differed from the low-expression group ($P < 0.05$), showing survival benefits. Moreover, compared with the WHO III group, the WHO II group was significantly different ($P = 0.029$) in terms of survival. In addition, the high *CCND1* expression group was significantly higher than the low-expression group ($P < 0.05$) based on the RS in the LR and SVM models. Our findings suggest that while the clinical model alone has good prognostic power, the model combining radiomic features with *CCND1* has a better clinical value.

Although radiomics models work well, our study has several limitations that may provide directions for future studies. First, all the data were obtained from public datasets (TCGA and TCIA), and the images were inevitably variable in quality, which may have influenced the analysis. Second, we only conducted research on *CCND1*; other biomarkers, such as *CCND2* and *CDK1*, are worthy of further study. Third, this research was a retrospective study with 149

TABLE 4. Correlation Between Radiomics Score and CCND1, Immune-Related Genes

Variable1	Variable2	Correlation	P value
CCND1	HHLA2	-0.37	2.80E-06
CCND1	TNFRSF14	-0.30	0.0003
CCND1	CD200R1	-0.18	0.0292
CCND1	ICOSLG	-0.17	0.0440
CCND1	CD28	0.18	0.0245
CCND1	TNFRSF9	0.24	0.0027
CCND1	LAG3	0.26	0.0014
CCND1	CD276	0.31	0.0001
CCND1	NRP1	0.32	5.77E-05
CCND1	RS	0.36	5.83E-06
RS	TIGIT	-0.17	0.0409
RS	TNFRSF8	0.16	0.0498
RS	TNFRSF9	0.30	0.0003
RS	CCND1	0.36	5.83E-06

CCND1, Cyclin D1; CD200R1, CD200 Receptor 1; CD276 Molecule; CD28, CD28 Molecule; HHLA2, HERV-H LTR-Associating 2; RS, radiomics model; ICOSLG, Inducible T Cell Costimulator Ligand; LAG3, Lymphocyte Activating 3; CD276, NRP1, Neuropilin 1; TNFRSF14, TNF Receptor Superfamily Member 14; TNFRSF9, TNF Receptor Superfamily Member 9

samples from TCIA; therefore, its generalizability must be further validated. Finally, radiomics analysis was based on manual segmentation by two radiologists. In other words, automated technology should be developed in further research to improve the reproducibility of radiomics analysis and reduce operator error.

CONCLUSION

In conclusion, *CCND1* expression levels could significantly influence the prediction and prognosis of patients with LGG. We constructed two radiomics-based models to effectively predict *CCND1* expression levels. Therefore, our model can be widely used as an effective method for non-invasive tumor characterization.

ETHICS APPROVAL AND CONSENT TO PARTICIPATE

Not applicable.

PATIENT CONSENT FOR PUBLICATION

Not applicable.

DECLARATION OF COMPETING INTEREST

The authors declare that they have no known competing financial interests or personal relationships that could have appeared to influence the work reported in this paper.

REFERENCES

- Ogino H, Taylor JW, Nejo T, et al. Randomized trial of neoadjuvant vaccination with tumor-cell lysate induces T cell response in low-grade gliomas. *J Clin Invest* 2022; 132(3):e151239. <https://doi.org/10.1172/jci151239>
- Louis DN, Perry A, Wesseling P, et al. The 2021 WHO classification of tumors of the central nervous system: a summary. *Neuro Oncol* 2021; 23(8):1231–1251. <https://doi.org/10.1093/neuonc/noab106>
- Haddad AF, Young JS, Oh JY, et al. The immunology of low-grade gliomas. *Neurosurg Focus* 2022; 52(2):E2. <https://doi.org/10.3171/2021.11.Focus21587>
- Salam R, Saliou A, Bielle F, et al. Cellular senescence in malignant cells promotes tumor progression in mouse and patient Glioblastoma. *Nat Commun* 2023; 14(1):441. <https://doi.org/10.1038/s41467-023-36124-9>
- Sanai N, Chang S, Berger MS. Low-grade gliomas in adults. *J Neurosurg* 2011; 115(5):948–965. <https://doi.org/10.3171/2011.7.Jns101238>
- Musgrove EA, Caldon CE, Barraclough J, et al. Cyclin D as a therapeutic target in cancer. *Nat Rev Cancer* 2011; 11(8):558–572. <https://doi.org/10.1038/nrc3090>
- Pestell RG. New roles of cyclin D1. *Am J Pathol* 2013; 183(1):3–9. <https://doi.org/10.1016/j.ajpath.2013.03.001>
- Sherr CJ, Roberts JM. Living with or without cyclins and cyclin-dependent kinases. *Genes Dev* 2004; 18(22):2699–2711. <https://doi.org/10.1101/gad.1256504>
- Liu J, Lin J, Wang X, et al. CCND1 amplification profiling identifies a subtype of melanoma associated with poor survival and an immunosuppressive tumor microenvironment. *Front Immunol* 2022; 13:725679. <https://doi.org/10.3389/fimmu.2022.725679>
- Du Q, Guo X, Wang M, et al. The application and prospect of CDK4/6 inhibitors in malignant solid tumors. *J Hemato Oncol* 2020; 13(1):41. <https://doi.org/10.1186/s13045-020-00880-8>
- Hosny A, Parmar C, Quackenbush J, et al. Artificial intelligence in radiology. *Nat Rev Cancer* 2018; 18(8):500–510. <https://doi.org/10.1038/s41568-018-0016-5>
- Huang EP, O'Connor JPB, McShane LM, et al. Criteria for the translation of radiomics into clinically useful tests. *Nat Rev Clin Oncol* 2023; 20(2):69–82. <https://doi.org/10.1038/s41571-022-00707-0>
- Chitalia RD, Rowland J, McDonald ES, et al. Imaging phenotypes of breast cancer heterogeneity in preoperative breast dynamic contrast enhanced magnetic resonance imaging (DCE-MRI) scans predict 10-year recurrence. *Clin Cancer Res* 2020; 26(4):862–869. <https://doi.org/10.1158/1078-0432.Ccr-18-4067>
- Chen M, Lu H, Copley SJ, et al. A novel radiogenomics biomarker for predicting treatment response and pneumotoxicity from programmed cell death-1 pathway inhibition in non-small cell lung cancer. *J Thorac Oncol* 2023; 18(6):718–730. <https://doi.org/10.1016/j.jtho.2023.01.089>
- Cui H, Sun Y, Zhao D, et al. Radiogenomic analysis of prediction HER2 status in breast cancer by linking ultrasound radiomic feature module with biological functions. *J Transl Med* 2023; 21(1):44. <https://doi.org/10.1186/s12967-022-03840-7>
- Wang P, He J, Ma X, et al. Applying MAP-MRI to identify the WHO grade and main genetic features of adult-type diffuse gliomas: a comparison of three diffusion-weighted MRI models. *Acad Radiol* 2023; 30(7):1238–1246. <https://doi.org/10.1016/j.acra.2022.10.009>
- Casale R, Lavrova E, Sanduleanu S, et al. Development and external validation of a non-invasive molecular status predictor of chromosome 1p/19q co-deletion based on MRI radiomics analysis of low grade glioma patients. *Eur J Radiol* 2021; 139:109678. <https://doi.org/10.1016/j.ejrad.2021.109678>
- Li ZZ, Liu PF, An TT, et al. Construction of a prognostic immune signature for lower grade glioma that can be recognized by MRI radiomics features to predict survival in LGG patients. *Transl Oncol* 2021; 14(6):101065. <https://doi.org/10.1016/j.tranon.2021.101065>
- Xiao Z, Yao S, Wang ZM, et al. Multiparametric MRI features predict the SYP gene expression in low-grade glioma patients: a machine learning-based radiomics analysis. *Front Oncol* 2021; 11:663451. <https://doi.org/10.3389/fonc.2021.663451>
- Xu C, Peng Y, Zhu W, et al. An automated approach for predicting glioma grade and survival of LGG patients using CNN and radiomics. *Front Oncol* 2022; 12:969907. <https://doi.org/10.3389/fonc.2022.969907>
- Kassambara A. (2017). Drawing Survival Curves using 'ggplot2' [R package survminer version 0.2.0].

22. Vivian J, Rao AA, Nothhaft FA, et al. Toil enables reproducible, open source, big biomedical data analyses. *Nat Biotechnol* 2017; 35(4): 314–316. <https://doi.org/10.1038/nbt.3772>
23. Wickham, H. (2009). Ggplot2: Elegant Graphics for Data Analysis. ggplot2: Elegant Graphics for Data Analysis.
24. Therneau, T.M., & Grambsch, P.M. (2013). Modeling Survival Data: Extending the Cox Model. *Modeling Survival Data: Extending the Cox Model*.
25. Miao YR, Zhang Q, Lei Q, et al. ImmuCellAI: a unique method for comprehensive T-cell subsets abundance prediction and its application in cancer immunotherapy. *Adv Sci (Weinh)* 2020; 7(7):1902880. <https://doi.org/10.1002/advs.201902880>
26. Hanzelmann S, Castelo R, Guinney J. GSVA: gene set variation analysis for microarray and RNA-seq data. *BMC Bioinformatics* 2013; 14:7. <https://doi.org/10.1186/1471-2105-14-7>
27. Phipson B, Lee S, Majewski IJ, et al. Robust hyperparameter estimation protects against hypervariable genes and improves power to detect differential expression. *Ann Appl Stat* 2016; 10(2):946–963. <https://doi.org/10.1214/16-AOS920>
28. Ritchie ME, Phipson B, Wu D, et al. limma powers differential expression analyses for RNA-sequencing and microarray studies. *Nucleic Acids Res* 2015; 43(7):e47. <https://doi.org/10.1093/nar/gkv007>
29. van Griethuysen JJM, Fedorov A, Parmar C, et al. Computational radiomics system to decode the radiographic phenotype. *Cancer Res* 2017; 77(21):e104–e107. <https://doi.org/10.1158/0008-5472.Can-17-0339>
30. Zhang Z, Gayle AA, Wang J, et al. Comparing baseline characteristics between groups: an introduction to the CBCgrps package. *Ann Transl Med* 2017; 5(24):484. <https://doi.org/10.21037/atm.2017.09.39>
31. Leijenaar RT, Carvalho S, Velazquez ER, et al. Stability of FDG-PET radiomics features: an integrated analysis of test-retest and inter-observer variability. *Acta Oncol* 2013; 52(7):1391–1397. <https://doi.org/10.3109/0284186x.2013.812798>
32. Hervey-Jumper SL, Zhang Y, Phillips JJ, et al. Interactive effects of molecular, therapeutic, and patient factors on outcome of diffuse low-grade glioma. *J Clin Oncol* 2023; 41(11):2029–2042. <https://doi.org/10.1200/jco.21.02929>
33. Zhang H. CCND1 silencing suppresses liver cancer stem cell differentiation through inhibiting autophagy. *Hum Cell* 2020; 33(1):140–147. <https://doi.org/10.1007/s13577-019-00295-9>
34. Ding H, Wang Y, Zhang H. CCND1 silencing suppresses liver cancer stem cell differentiation and overcomes 5-Fluorouracil resistance in hepatocellular carcinoma. *J Pharmacol Sci* 2020; 143(3):219–225. <https://doi.org/10.1016/j.jphs.2020.04.006>
35. Valla M, Klæstad E, Ytterhus B, et al. CCND1 amplification in breast cancer -associations with proliferation, histopathological grade, molecular subtype and prognosis. *J Mammary Gland Biol Neoplasia* 2022; 27(1):67–77. <https://doi.org/10.1007/s10911-022-09516-8>
36. Sushma PS, Jamil K, Udaykumar P, et al. Analysis of CCND1 protein and circulatory antioxidant enzyme activity association in oral squamous cell carcinoma. *Saudi J Biol Sci* 2021; 28(12):6987–6991. <https://doi.org/10.1016/j.sjbs.2021.07.085>
37. Ying Y, Li J, Xie H, et al. CCND1, NOP14 and DNMT3B are involved in miR-502-5p-mediated inhibition of cell migration and proliferation in bladder cancer. *Cell Prolif* 2020; 53(2):e12751. <https://doi.org/10.1111/cpr.12751>
38. Jeon S, Kim Y, Jeong YM, et al. CCND1 splice variant as a novel diagnostic and predictive biomarker for thyroid cancer. *Cancers (Basel)* 2018; 10(11):437. <https://doi.org/10.3390/cancers10110437>
39. Chen X, Zhao T, Li L, et al. CCND1 G870A polymorphism with altered cyclin D1 transcripts expression is associated with the risk of glioma in a Chinese population. *DNA Cell Biol* 2012; 31(6):1107–1113. <https://doi.org/10.1089/dna.2011.1521>
40. Li J, Qiu Z, Cao K, et al. Predicting muscle invasion in bladder cancer based on MRI: A comparison of radiomics, and single-task and multi-task deep learning. *Comput Methods Programs Biomed* 2023; 233:107466. <https://doi.org/10.1016/j.cmpb.2023.107466>
41. Feng S, Yin J. Radiomics of dynamic contrast-enhanced magnetic resonance imaging parametric maps and apparent diffusion coefficient maps to predict Ki-67 status in breast cancer. *Front Oncol* 2022; 12:847880. <https://doi.org/10.3389/fonc.2022.847880>
42. Yue X, He X, He S, et al. Multiparametric magnetic resonance imaging-based radiomics nomogram for predicting tumor grade in endometrial cancer. *Front Oncol* 2023; 13:1081134. <https://doi.org/10.3389/fonc.2023.1081134>
43. Liao CY, Lee CC, Yang HC, et al. Predicting survival after radiosurgery in patients with lung cancer brain metastases using deep learning of radiomics and EGFR status. *Phys Eng Sci Med* 2023; 46(2):585–596. <https://doi.org/10.1007/s13246-023-01234-7>
44. Li XM, Liu SP, Liu DM, et al. Identification of disulfidptosis-related genes and immune infiltration in lower-grade glioma. *Open Med (Wars)* 2023; 18(1):20230825. <https://doi.org/10.1515/med-2023-0825>
45. Xiao F, Zhu H, Guo Y, et al. CIA-II is associated with lower-grade glioma survival and cell proliferation. *CNS Neurosci Ther* 2023; 30(2):e14340. <https://doi.org/10.1111/cns.14340>
46. Zhu Q, Liu Z, Cheng X, et al. ZNF480 influences the prognosis, pathogenesis, and immune microenvironment in patients with lower-grade glioma. *Heliyon* 2023; 9(7):e18185. <https://doi.org/10.1016/j.heliyon.2023.e18185>
47. Chen W, Gao C, Hu C, et al. Risk stratification and overall survival prediction in advanced gastric cancer patients based on whole-volume MRI radiomics. *J Magn Reson Imaging* 2023; 58(4):1161–1174. <https://doi.org/10.1002/jmri.28621>
48. Boot PA, Mes SW, de Bloeme CM, et al. Magnetic resonance imaging based radiomics prediction of Human Papillomavirus infection status and overall survival in oropharyngeal squamous cell carcinoma. *Oral Oncol* 2023; 137:106307. <https://doi.org/10.1016/j.oraloncology.2023.106307>
49. Ming W, Li F, Zhu Y, et al. Unsupervised analysis based on DCE-MRI radiomics features revealed three novel breast cancer subtypes with distinct clinical outcomes and biological characteristics. *Cancers (Basel)* 2022; 14(22):5507. <https://doi.org/10.3390/cancers14225507>
50. Wan Y, Zhou S, Zhang Y, et al. Radiomic analysis of contrast-enhanced MRI predicts DNA copy-number subtype and outcome in lower-grade gliomas. *Acad Radiol* 2022; 29(9):e189–e196. <https://doi.org/10.1016/j.acra.2021.10.014>